



Contents lists available at ScienceDirect

Arabian Journal of Chemistry

journal homepage: www.ksu.edu.sa

Original article

Blue coke-based activated carbon adsorbents: Insights into the efficiency and mechanism of methyl blue removal

Yunxuan Luoyang^a, Hua Wang^{a,b,*}, Wang Yong^c, Jian Li^a, Xia Li^a, Han Shenghu^d, Nie Ying^e, Zhang Guotao^a^a College of Chemistry and Chemical Engineering, Yulin University, Yulin City 719000, China^b Shaanxi Provincial Key Laboratory of Clean Utilization of Low-Modified Coal, Yulin University, Yulin City 719000, China^c Xiaojihan Coal Mine, Shaanxi Huadian Yuheng Coal Electricity Limited Liability Company, Yulin City 719000, China^d Shaanxi Yanchang Petroleum Group Co Ltd., Shaanxi, Yulin City 719000, China^e Shaanxi Yuneng Chemical Materials Limited Company, Yulin City 719000, China

ARTICLE INFO

Keywords:

Blue coke
Adsorption isotherm
Methylene blue
Adsorption kinetics
Adsorption thermodynamics

ABSTRACT

In this study, a systematic analysis was conducted to investigate the efficiency and mechanism of methylene blue (MB) removal from water using blue coke-based activated carbon (AC) as an adsorbent. The investigation encompassed several critical parameters, including adsorbent dosage, contact time, pH, temperature, initial MB concentration, and the regeneration capacity of the adsorbent. The adsorption mechanism of MB by AC was elucidated through instrumental analysis and theoretical models such as adsorption kinetics, isotherm models, and thermodynamic analysis. The experimental results demonstrated several key findings: the removal efficiency of MB increased with the adsorbent dosage, although the unit adsorption capacity decreased; the removal rate of MB rose rapidly with increasing contact time and reached equilibrium after 90 min; the highest removal efficiency was achieved at pH 6; the adsorption capacity increased with higher initial MB concentrations. The adsorption kinetics conformed to the pseudo-second-order model, indicating that chemical adsorption was the predominant control step. The adsorption process was identified as a spontaneous reaction, with the Langmuir model suggesting a maximum adsorption capacity of 2040.696 mg/g at 318 K. Furthermore, AC exhibited an abundant mesoporous structure and surface functional groups, contributing to the efficient removal of MB. The adsorption mechanism involved pore-filling, hydrogen bonding, π - π interactions, and electrostatic attraction. Additionally, AC demonstrated excellent regeneration performance. These findings suggest that AC prepared from blue coke holds significant potential for industrial applications in MB removal, owing to its high removal efficiency, low cost, and good regenerative properties, making it highly valuable for practical use.

1. Introduction

MB is an organic dye widely used in the textile, paper, printing, and pharmaceutical industries (Malatji et al., 2021). It possesses high stability and is resistant to degradation, allowing it to persist in aquatic environments for extended periods (Liu, Omer, and Ouyang, 2017). The presence of MB in water bodies can cause toxicity in fish, plankton, and other aquatic organisms, leading to physiological dysfunction and even death (Sen, 2014; Arabzadeh et al., 2023). Consumption of contaminated water by humans can result in vomiting, mutations, cancer, respiratory issues, diarrhea, eye burns, nausea, shock, cyanosis, jaundice,

and tissue necrosis (Makhado et al., 2017). Long-term exposure to low concentrations of MB may cause metabolic disorders, organ damage, and genetic toxicity in organisms (Makhado et al., 2017). Furthermore, MB can impede photosynthesis, bioaccumulate in marine organisms, and induce biomagnification effects within the ecological environment (Emmanuel and Adesibikan, 2021). To protect water resources and the ecological environment, various countries have established stringent regulations on the discharge of dyes such as MB into water bodies, typically monitored through parameters like chemical oxygen demand.

A variety of water treatment technologies have been developed to meet the emission standards for MB dye wastewater discharge, including

Peer review under responsibility of King Saud University.

* Corresponding author at: College of Chemistry and Chemical Engineering, Yulin University, Chongwen Road No.51, Yulin City 719000, Shaanxi Province, China.

E-mail address: 99452715@qq.com (H. Wang).<https://doi.org/10.1016/j.arabjc.2024.105898>

Received 23 March 2024; Accepted 6 July 2024

Available online 14 July 2024

1878-5352/© 2024 The Author(s). Published by Elsevier B.V. on behalf of King Saud University. This is an open access article under the CC BY license (<http://creativecommons.org/licenses/by/4.0/>).

adsorption (Li et al., 2019), flocculation (Teixeira et al., 2022), membrane separation (Parakala, Moulik, and Sridhar, 2019), chemical oxidation (He et al., 2016), electrochemical degradation (Hu et al., 2022), photocatalytic degradation (Chang et al., 2024), and biodegradation (Nabilah et al., 2023). Among these methods, adsorption stands out for its flexibility in design, cost-effectiveness, ease of operation and absence of secondary pollution (Jawad et al., 2022; Küçük, 2023; Sahu et al., 2022). Therefore, the search for efficient, economical and environmentally friendly adsorbents for wastewater treatment is particularly important.

Blue coke is an innovative coke material prepared by a low-temperature dry distillation process of high-quality Jurassic weakly viscous coal produced from the Shenfu coal field at a strictly controlled condition of about 600 °C (Lu et al., 2013). Blue coke is noted for its high fixed coke content, high specific electrical resistance and remarkable chemical activity, as well as environmentally friendly attributes such as low ash, sulphur and phosphorus content (Feng, Xu, and Wang, 2024). These combined properties augur well for the promising and significant application of blue coke in industrial applications (Feng and Xu, 2020). Nevertheless, the potential application value of blue coke powder with particle size less than 3 mm has not been fully developed and utilised due to its limitations in traditional industrial applications (Tian et al., 2022). However, based on its unique physicochemical properties, blue coke powder is considered an excellent precursor material for the preparation of high quality activated carbon.

Blue coke based activated carbon is expected to be a new type of adsorbent material with abundant resources, low price and excellent adsorption performance. The aim of this study was to evaluate the treatment effect and application potential of blue coke-based activated carbon in the simulated wastewater treatment of MB dye through systematic experimental studies and mechanistic analyses. By exploring the relationship between the structural properties and adsorption performance of the blue coke-based activated carbon under different preparation conditions, the mechanism of adsorption was revealed to provide theoretical basis and technical support for its application in practical wastewater treatment.

2. Experimental methods

2.1. Materials and chemicals

The blue coke powder (LC) utilized in this experiment was supplied by the chemical plant located in Shaanxi, China. KOH, HNO₃, and MB (C₁₆H₁₈ClN₃S) were supplied by Tianjin Kemiou Chemical Reagent Co., Ltd.. All of the compounds were analytically pure and utilized directly without any additional purification.

2.2. Preparation of adsorbent

Samples were prepared with reference to previously published literature (Wang et al., 2023). LC, having passed through a 200-mesh sieve, was subjected to ultrasonic cleaning with water and subsequently dried in a hot air oven at 105 °C. The pre-treated LC was mixed with potassium hydroxide at a mass ratio of 1:4, and then placed in a tube furnace under nitrogen atmosphere at 800 °C for 2 h. The product was washed with 10 % hydrochloric acid (v/v) three times, and then washed with deionised water to neutral. The pyrolysis products were washed three times with 10 % hydrochloric acid (v/v) and then washed with deionised water until neutral to obtain the AC sample. The AC sample was stirred in 30 % nitric acid (v/v) at a solid-liquid ratio of 1:20 (g:ml) for 6 h at room temperature, and the filtrate was washed with water until neutral and then dried to obtain the ACN sample.

2.3. Material characterization

Field emission scanning electron microscopy (FESEM, SIGMA 300,

Germany); X-ray photoelectron spectroscopy (XPS, Thermo Scientific K-Alpha, USA); Fourier transform infrared spectroscopy (FTIR, TENSOR 27, Bruker, Germany); UV-Vis spectrophotometer (Shanghai Jing Hua, China); and PHS-3C acidity meter (Shanghai Lei Magnetic, China) are the principal tools and equipment used for characterizing material properties.

2.4. Adsorption experiment

A number of parameters, including the adsorbent dosage (20–150 mg), adsorption period (0–240 min), initially concentration of MB (0–700 mg/L), pH value (2–10), and temperature (298–318 K), were investigated to determine the factors influencing the adsorption effectiveness of MB. A certain volume of solution was obtained for the adsorption experiment, and after filtering through a 0.45 μm membrane, the absorbance was measured at a wavelength of 665 nm. The capacity for adsorption (q_t) and the removal effectiveness (R) of MB were calculated using formulas (1) and (2), respectively.

$$q_t = \frac{V(C_0 - C_t)}{m} \quad (1)$$

$$R = \frac{C_0 - C_t}{C_0} \times 100\% \quad (2)$$

The formulas show that the MB solution's volume is V (L), and the adsorbent's mass is m (g), and C₀ and C_t (mg·L⁻¹) are the initial and time t concentrations of MB, respectively.

2.5. Regeneration experiment of AC

The adsorbed AC was subjected to desorption and regeneration by immersing it in an anhydrous ethanol solution with a 1 g/L solid-to-liquid ratio. The mixture was constantly stirred for six hours followed by a solid-liquid segregation achieved via centrifugation. The sample was then recycled, and the removal efficiency of MB determined after each cycle of adsorption-regeneration.

2.6. Data analysis methods

All adsorption experimental data were averaged from the results of three replicate experiments. The adsorption models and equations employed for adsorption kinetics, adsorption isotherms, and adsorption thermodynamic analyses are as follows:

- Adsorption kinetics models

First-order pseudokinetic model:

$$\ln(q_e - q_t) = \ln q_e - k_1 t \quad (3)$$

Second-order pseudokinetic model:

$$\frac{t}{q_t} = \frac{1}{k_2 q_e^2} + \frac{t}{q_e} \quad (4)$$

Intraparticle diffusion model:

$$q_t = k_{df} t^{0.5} + C \quad (5)$$

Where the equilibrium is represented by q_e (mg·g⁻¹). The rate constants for First-order and Second-order pseudokinetic model are, respectively, k_1 (min⁻¹) and k_2 (g·mg⁻¹·min⁻¹). Intraparticle diffusion's rate constant is k_{df} (mg·g⁻¹·min^{1/2}). A constant associated with the thickness of the boundary layer is denoted by C (mg·g⁻¹).

- Adsorption isotherm

Langmuir model:

$$\frac{C_e}{q_e} = \frac{C_e}{q_m} + \frac{1}{q_m K_L} \quad (6)$$

$$R_L = \frac{1}{1 + K_L \times C_0} \quad (7)$$

Freundlich model:

$$\ln q_e = \ln K_F + \frac{1}{n} \ln C_e \quad (8)$$

Where the constants for the Freundlich and Langmuir equilibriums are, respectively, $K_F(\text{mg} \cdot \text{g}^{-1})$ and $K_L(\text{L} \cdot \text{mg}^{-1})$. An empirical value is the parameter n .

• Thermodynamics

The enthalpy value (ΔH), the Gibbs free energy value (ΔG), and the entropy change (ΔS) thermodynamic parameters are used to calculate the thermal characteristics of the adsorption process. For this, the following formulas are employed:

$$\ln K_d = \frac{q_e}{C_e} \quad (9)$$

$$\ln K_d = \frac{\Delta S}{R} - \frac{\Delta H}{RT} \quad (10)$$

$$\Delta G = -RT \ln K_d \quad (11)$$

The graph's slope and intercept can be used to determine ΔH and ΔS . R is the universal gas constant ($8.314 \text{ J}/(\text{mol} \cdot \text{K})$), T is the absolute temperature (K), and K_d is the thermodynamic equilibrium constant.

3. Results and discussion

3.1. Factors affecting adsorption effectiveness

3.1.1. Adsorption time

Fig. 1a illustrates how the two adsorbents' capacities to absorb MB change over time. Between 0 and 90 min, the removal efficiency and adsorption capacity of AC and ACN for MB improve rapidly, with minimal change observed after 120 min. Within the first 90 min, AC demonstrates higher removal efficiency and adsorption capacity for MB compared to ACN. However, this advantage diminishes after 120 min, indicating that during the initial stage of adsorption, AC initially provides more active sites conducive to rapid MB adsorption, leading to a higher rate of adsorption. Over time, the availability of these active adsorption sites decreases, resulting in a slower MB adsorption rate. Eventually, both AC and ACN reach adsorption equilibrium and the adsorption rate stabilizes. After 120 min, there is no significant difference in MB removal efficiency between AC and ACN. This can be attributed to the fact that with a sample size of 250 mg and a 300 mg/L MB concentration, there is a sufficient amount of MB available for both adsorbents to effectively adsorb, leaving no additional MB in the aqueous solution for further adsorption.

3.1.2. pH value

The results of an investigation into the efficacy of AC and ACN for MB removal at various pH levels are displayed in Fig. 1b. In the pH range of 2 to 10, it was found that AC consistently performed better than ACN in terms of MB removal efficiency. At pH 6, both adsorbents showed the best removal efficacy for MB. The pH of the solution can impact the surface charge and other properties of the adsorbent materials. A material's surface charge can be ascertained under various pH conditions using its pH_{zpc} value: when $\text{pH} < \text{pH}_{\text{zpc}}$, the material's surface charge is positive, and at $\text{pH} > \text{pH}_{\text{zpc}}$, it is negative (Guzel et al., 2017). The pH_{zpc} values of AC and ACN are 7.46 and 8.18, respectively (Wang et al., 2023). Thus, it can be said that throughout the pH range of 2–6, positive

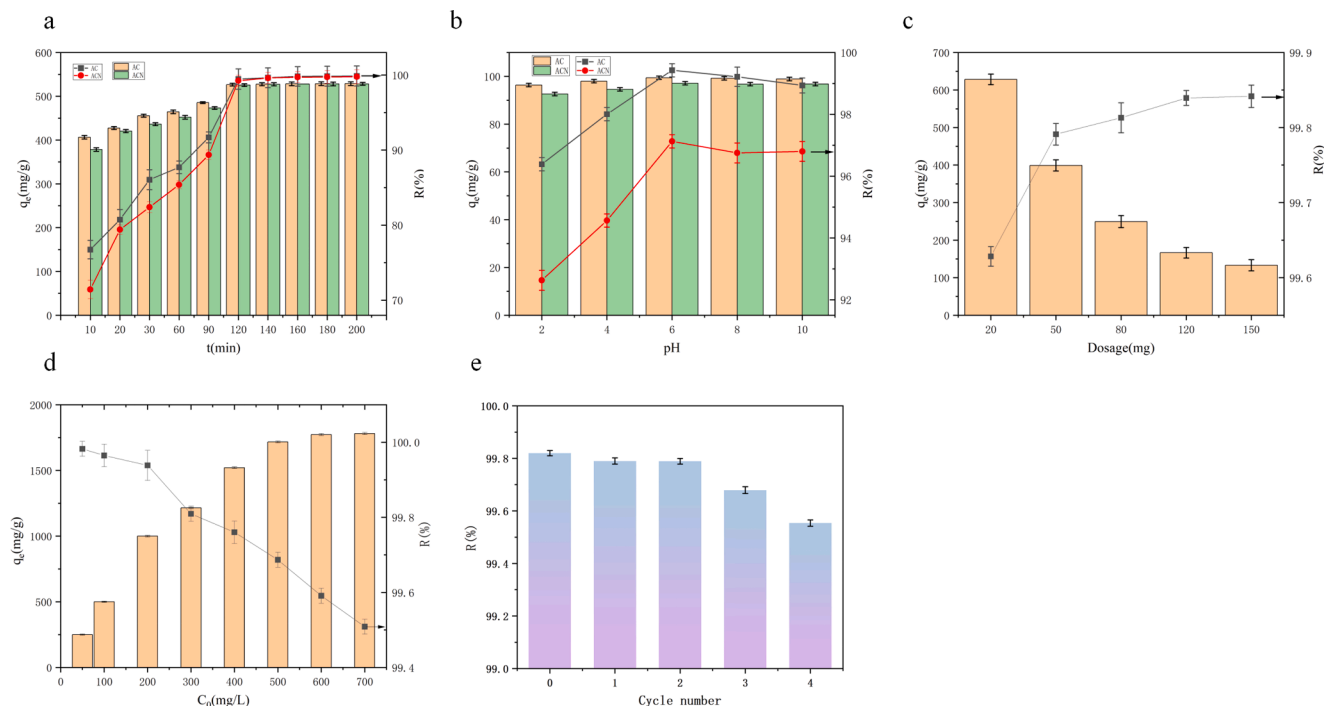


Fig. 1. (a)Effect of time on removal capacity of MB by AC and ACN($C_0 = 300 \text{ mg/L}$; dosage = 250 mg, and $V=500 \text{ mL}$). (b)Effect of pH on the removal capacity of MB by AC and ACN($C_0 = 200 \text{ mg/L}$, dosage = 10 mg, and $V=50 \text{ mL}$). (c)Effect of adsorbent dosage on removal capacity of MB by AC($C_0 = 400 \text{ mg/L}$ and $V=50 \text{ mL}$). (d)Effect of initial concentration on removal capacity of MB by AC(dosage = 10 mg and $V=50 \text{ mL}$). (e)The effect of the number of reuse cycles on the removal capacity of MB by AC($C_0 = 200 \text{ mg/L}$, dosage = 10 mg, and $V=50 \text{ mL}$).

charges are present on both AC and ACN surfaces.

Lower pH values make the solution more acidic, and higher acidity increases the H^+ content in the solution. More positive charges are present on the adsorbent surface as a result of this protonation, which increases the electrostatic repulsion of the MB cations and prevents their adsorption (Elsherbiny, El-Hefnawy, and Gemeay, 2017). Furthermore, in acidic environments, H^+ competes with the adsorbent's active sites for the MB cations, reducing the adsorption capacity (Miao et al., 2021). This explains why the MB removal efficiency trend improves as the pH value rises in the pH 2–6 range. Positive charges on the material surface diminish as the pH of the solution rises. The surface's negative charges allow the MB cations to more easily adsorb when pH is higher than pH_{zpc} . Contrary to predictions, Fig. 1b shows that removal efficiency tends to decrease as pH rises. The reason for this could be that the solution's OH^- ions, which affect the adsorbent's active sites (such COO^- or phenolic hydroxyl groups), impact the electrostatic interaction between them and MB (Bai et al., 2023b). More research on AC's adsorption characteristics is necessary given its superior MB elimination performance.

3.1.3. Dosage

Fig. 1c shows the findings of an investigation into the impact of AC dosage on MB removal efficiency. The elimination efficiency of MB exhibited a rising trend with a dosage increase, and its growth rate eventually leveled off. This suggests that if the dosage is increased, the number of adsorbed sites on the surface of the adsorbent increases in addition, offering a enough number of active sites to remove MB from the solution (Wang et al., 2020). In contrast to the removal efficiency, the adsorbent's unit adsorption capacity dropped as the dosage increased, suggesting a decrease in the adsorbent's active site use. The reduced utilization of active sites is the reason for the decline in the unit adsorption capacity of AC for MB. Using a large amount of adsorbent can cause adsorbent particles to aggregate or increase competition for adsorption (Yong et al., 2019), which will ultimately prevent AC's active sites from being fully utilized. Even though adding more AC to MB-containing solutions can somewhat increase the effectiveness of MB elimination, it would result in the wastage of AC. Therefore, for optimal results, it is advised to apply the appropriate amount of AC.

3.1.4. The initial MB concentration

The results of an investigation into the impact of the initial concentration of MB on the adsorption performance of AC are displayed in Fig. 1d. The effectiveness of MB removal decreased as the initial concentration of MB was elevated from 50 mg/L to 700 mg/L. In contrast, the adsorption capacity of MB increased from 249.95 mg/g to 1872.64 mg/g. This is because a higher initial concentration can enhance the mass transfer rate and improve the AC's ability to adsorb MB (Bello et al., 2008). As the initial concentration of MB increases, the driving force for mass transfer increases, providing more opportunities for contact between MB and the surface active sites of AC. This leads to a rise in the use of the AC's active sites, as manifested by an expansion of AC's unit adsorption capacity. As the initial concentration of MB continues to increase, when all the active sites of AC are exhausted, the unit adsorption capacity no longer increases with the solution's initial concentration increasing until AC's maximal adsorption capacity for MB is reached. Due to the limitation of the adsorbent dosage, the adsorption sites that AC can provide are limited. The efficacy of MB removal decreases when the initial concentration of MB increases and AC is unable to supply enough active sites for MB adsorption. The adsorption equilibrium conditions limit the concentration of MB in the solid-liquid phase.

3.1.5. Regeneration and recycling

The adsorption efficiency of the adsorbent decreases with increasing usage. This decrease is mainly due to the damage or occlusion of the structure of the pores on the surface of the adsorbent after many cycles

of use, leading to a decrease in the availability of active sites and specific surface area (Ul Alamin et al., 2021). Therefore, the reusability of adsorbents is a key indicators to evaluate their performance. High reusability significantly improves the cost-effectiveness of adsorbents. Fig. 1e shows the results of cycling experiments using AC as an adsorbent after regeneration with anhydrous ethanol. The data show that the adsorption efficacy of the adsorbent decreases only slightly after the regeneration treatment. Thus, AC shows excellent stability and superior reusability, highlighting its advantages as an efficient adsorbent material.

3.2. Adsorption kinetics analysis

The entire adsorption process may be divided into three stages (Fig. 2a): the rapid (0–60 min), slow (60–120 min), and equilibrium (after 120 min). The large concentration differential of MB between the solution and the AC surface, which produces a significant mass transfer driving force, is primarily responsible for the faster adsorption rate observed in the rapid adsorption stage. However over time, the solution's and the AC surface's differences in MB concentration decrease, which causes the adsorption rate to steadily drop. Furthermore, the adsorption of MB on AC is slowed down by the repulsion that arises from MB's binding to an abundance of active sites on the AC surface. This repulsion increases the diffusion resistance that prevents the adsorbate from entering the pores (Yusop et al., 2021). The adsorption steadily gets closer to equilibrium as the surface of the AC's active sites fill up.

The adsorption kinetics were examined in order to gain a deeper understanding of the adsorption process and mechanism. The kinetic data were fitted using pseudo first and pseudo second order kinetic models; the fitting curves are displayed in Fig. 2a, and the computed parameters are included in Table 1.

The two kinetic models have high correlation coefficients (R^2) that exceed 0.956, as shown in Table 2. Nearly identical to the experimental value of 276.5 mg/g are the computed equilibrium adsorption capacities from both models, which are 279.8 mg/g and 279.7 mg/g, respectively. This implies that both chemical and physical adsorption properties are involved in the adsorption of MB onto AC (Deng et al., 2022).

The intra-particle diffusion model provides a more realistic description of the adsorption process. Consequently, the intra-particle diffusion model was also used to fit the contact time data in this study. This linear fitting is shown in Fig. 2b, and the obtained parameters are listed in Table 2. The fact that none of the three fitting curves cross the origin implies that there are other rate-limiting phases besides intra-particle diffusion and that both surface adsorption and intra-particle transport play significant roles in the adsorption process. The adsorption process comprises three steps: firstly, from the liquid film to the external surface of AC, MB diffuses fastest, with the lowest constant C value and the highest diffusion rate constant (K_{df1}); secondly, MB is transferred through the adsorbent's internal pores; and thirdly, MB is adsorbed and desorbs between the active sites on AC, reaching the equilibrium stage, with the lowest K_{df3} value and the highest C value (Khasri, Bello, and Ahmad, 2018). It's important to note that the diffusion rate constant K_{df1} is significantly greater than K_{df2} and K_{df3} , suggesting that the interface is where MB is largely adsorbed (Han et al., 2022). A larger C value indicates a bigger influence of the boundary layer thickness and slower MB adsorption rate. The C value tells us how thick the boundary layer is. This information is derived from the quantity of active sites covered by MB on the surface of the AC (Sundaran et al., 2019). As a result, the third stage of the overall adsorption process is the rate-controlling step.

3.3. Adsorption isotherm analysis

As shown in Fig. 3a, the ability of MB absorbed on AC rises with temperature at the same initial concentration. This suggests that MB adsorbs endothermically on AC (Vasiraja, Prabhakar, and Joshua,

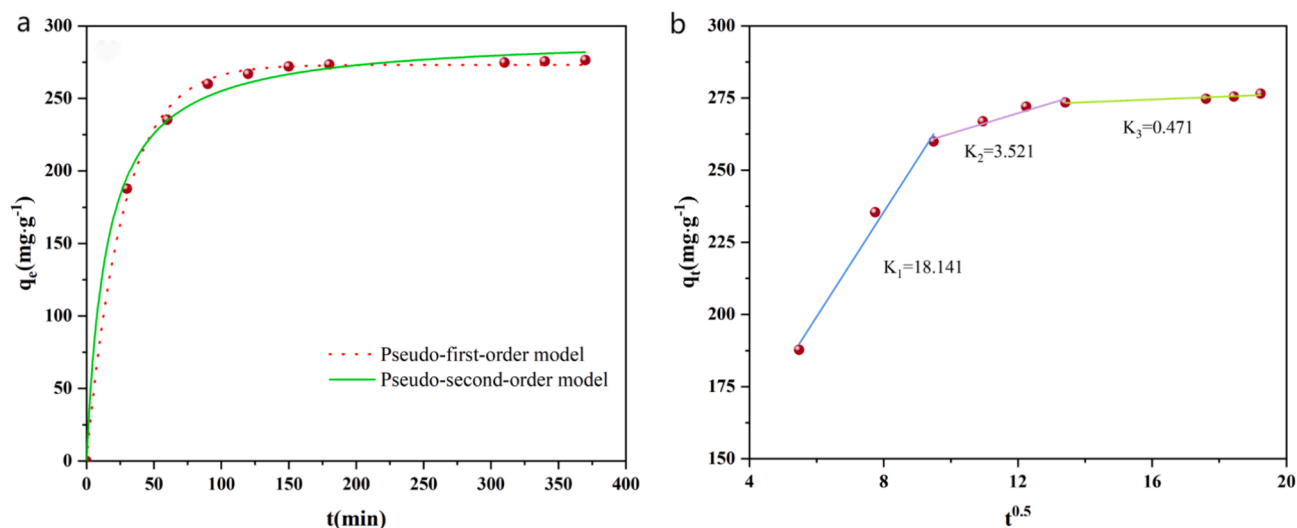


Fig. 2. (a) Fitting curves of pseudo-first-order and pseudo-second-order kinetic models, and (b) fitting curve of the internal diffusion model.

Table 1

The kinetic parameters of MB adsorption on AC.

AC	Pseudo-first order kinetic model				Pseudo-second-order dynamics		
C_0 (mg·L ⁻¹)	$q_{e(\text{exp})}$ (mg·g ⁻¹)	$q_{e(\text{cal})}$ (mg·g ⁻¹)	k_1 (min)	R^2	$q_{e(\text{cal})}$ (mg·g ⁻¹)	k_2 (mg·g ⁻¹ ·min ⁻¹)	R^2
350	276.5	279.8	0.013	0.956	279.7	3.51×10^{-3}	0.992

Table 2

The parameters of the intraparticle diffusion model for the adsorption of MB on AC.

C_0 (mg·L ⁻¹)	k_{df1} (mg·g ⁻¹ ·min ^{-1/2})	C (mg·g ⁻¹)	R^2	k_{df2} (mg·g ⁻¹ ·min ^{-1/2})	C (mg·g ⁻¹)	R^2	k_{df3} (mg·g ⁻¹ ·min ^{-1/2})	C (mg·g ⁻¹)	R^2
350	18.141	90.389	0.989	3.520	227.501	0.953	0.470	266.952	0.886

2023). With increasing starting concentration, temperature has a greater effect on AC's adsorption ability for MB; however, this difference gradually stabilizes. This can be explained by the following analysis: at lower initial concentrations, there is little variation in MB concentration between the solid and liquid phases, and temperature has little effect on mass transfer. The influence of temperature, however, becomes increasingly noticeable as the concentration gradient rises, and this difference stabilizes when the solute adsorption equilibrium between the liquid and solid phases is attained.

Adsorption isotherms are crucial instruments for determining an adsorbent's maximum adsorption capacity and comprehending how adsorption works. Fig. 3b and 3c show the adsorption isotherm values fitted with the Freundlich and Langmuir models, respectively. Table 3 provides a summary of the fitted parameters. It is evident that the Langmuir model's correlation coefficients (R^2) are higher than the Freundlich model's at various temperatures. As a result, the Langmuir adsorption model, which suggests that MB adsorption on AC occurs as monolayer adsorption process, and the highest adsorption capacity of AC for MB at 318 K is 2040.696 mg/g (Table 3). A reversible adsorption process is indicated by the separation factor (R_L) values from the Langmuir model at various temperatures (Table 3), which range from 0 to 1 (Somyanonthanakun et al., 2023). Table 4 compiles the adsorption capacities of various adsorbents for MB as reported in the literature. Analysis indicates that AC exhibits an adsorption capacity significantly higher than other adsorbents, demonstrating its superior adsorption performance.

3.4. Thermodynamic analysis

The results of the thermodynamic calculations are shown in Table 5.

It can be observed that the values of ΔG at temperatures of 298 K, 308 K, and 318 K are -22.610, -23.032, and -85.869 kJ/mol, respectively, indicating that the adsorption of MB on AC is spontaneous. As the temperature increases, the values of ΔG decrease, indicating that the adsorption of MB on AC becomes more favorable (Huang et al., 2018). Fig. 3d shows the thermodynamic fitting curves of AC at the three adsorption temperatures. The calculated ΔH for the adsorption of MB on AC is 4.781 kJ/mol, further confirming that the adsorption of MB on AC is an endothermic reaction. The ΔS for this adsorption process is 91.936 J/(mol·K), indicating an increase in entropy during the adsorption equilibrium of MB on AC. This suggests that the system tends to stabilize due to the arrangement and recombination of MB molecules at the solid-liquid interface of AC (Basta et al., 2019).

3.5. Reasons for superior adsorption performance of AC compared to ACN for MB

After analyzing the data in Sections 3.1.1 and 3.1.2, we found that AC exhibited superior performance in the removal of MB compared to ACN. Comparison of FESEM images (Fig. 4) of AC and ACN with MB adsorbed under the same adsorption conditions reveals that more lamellar structures were formed on the surface of AC after the adsorption of MB (Fig. 4a), whereas fewer corresponding structures were formed on ACN (Fig. 4b). In addition, most of the pores of AC were covered by adsorbed MB, which further verified the higher capacity of AC in adsorbing MB.

According to the findings from a BET analysis in a prior study (Wang et al., 2023), although the number of micropores and the specific surface area of AC were found to be smaller in comparison to those of ACN, the mesopore volume of AC within the pore size range of 2–4 nm exhibited a

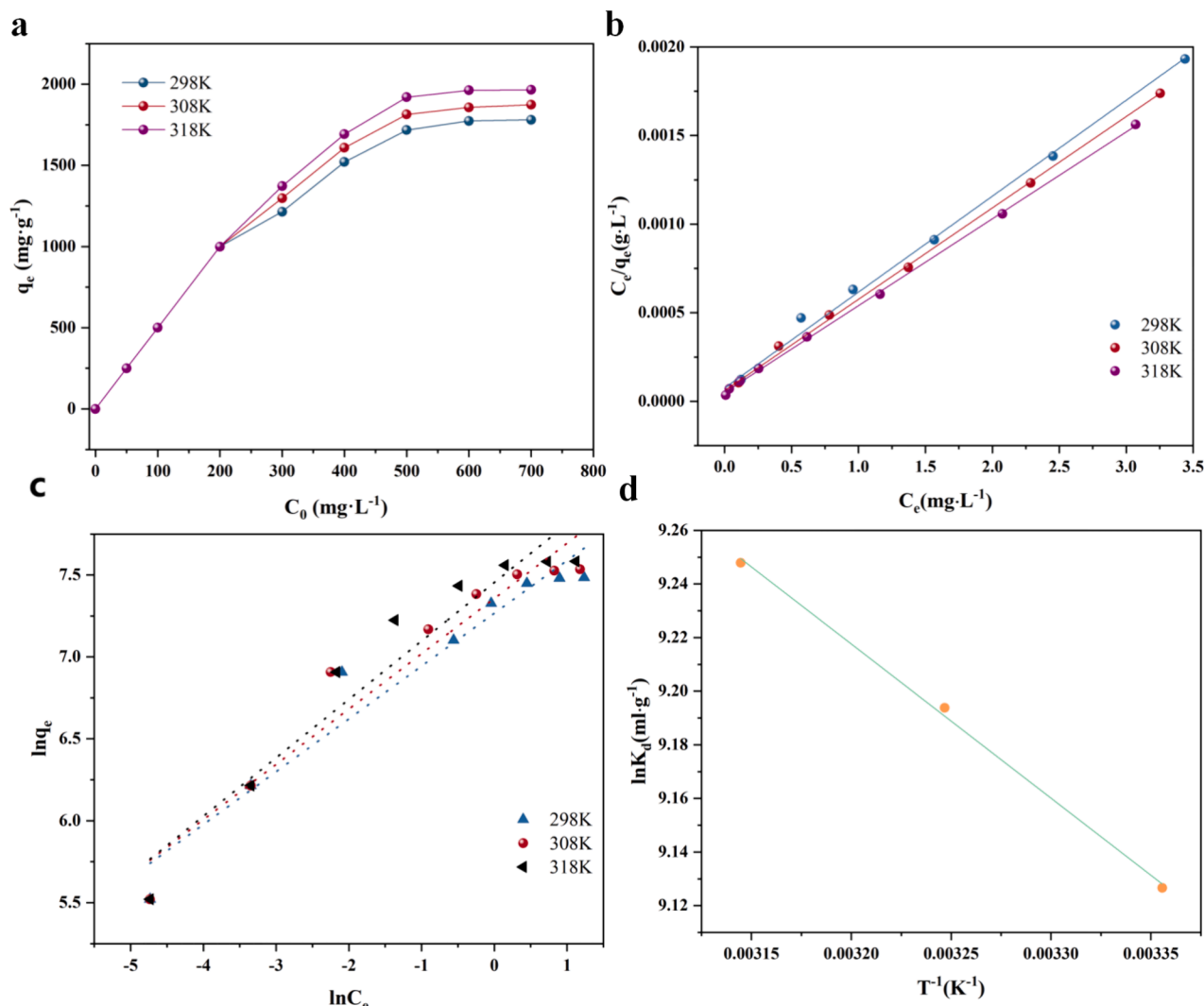


Fig. 3. (a) Effect of temperature on adsorption capacity of MB by AC (dosage = 10 mg and V=50 mL). (b) Fitting curve of the Langmuir model. (c) Fitting curve of the Freundlich model. (d) Fitting curve of the thermodynamic model.

Table 3

The adsorption isotherm parameters of MB adsorption on AC.

AC	Langmuir				Freundlich		
	K_L (L/mg)	q_{max} (mg/g)	R_L ($\times 10^{-4}$)	R^2	K_F (mg ¹⁻ⁿ ·Ln ⁻ⁿ ·g ⁻¹)	n	R^2
298 K	7.183	1847.787	1.99 ~ 27.76	0.996	1430.315	3.103	0.945
308 K	8.558	1939.488	1.67 ~ 23.31	0.998	1565.546	2.964	0.936
318 K	9.797	2040.696	1.46 ~ 20.37	0.999	1725.376	2.805	0.926

contrary trend. This pore structure characteristic of AC was not favorable for the adsorption of hexavalent chromium ions, but it was beneficial for the adsorption of MB. Since the diameter of the organic molecules of MB is larger than that of the hexavalent chromium inorganic salt ions, the screening effect of the micropores actually limits the adsorption of MB. Although ACN has a smaller average pore size and larger specific surface area, as well as a more developed microporous structure, which should supposedly provide more adsorption sites. Therefore, the experimental data suggest that the pore size structure of AC is more suitable for MB adsorption and removal.

By analyzing the FTIR (Fig. 5a), It can be observed that the wave numbers and peak intensities of the functional groups representing amino (Mani et al., 2023) (3493 cm⁻¹), hydroxyl (Mani et al., 2023) (3425 cm⁻¹ and 1213 cm⁻¹), carboxylic acid lactone group C=O and C-O-C (Bouchelkia et al., 2023) (1719 cm⁻¹) differed before and after the adsorption of MB by AC, indicating that N-containing and O-containing functional groups are involved in the adsorption process of MB. The difference in these functional groups in the AC and ACN structures, in addition to the sieving effect, is another key factor contributing to the difference in MB adsorption.

Oxygen-containing functional groups confer hydrophilicity to carbon materials (Zheng et al., 2023), thus enhancing the removal of MB. The FTIR revealed the differences in the types of oxygen-containing functional groups of LC, AC, and ACN, and Fig. 5b further showed that the O/C ratios of the three materials were also significantly different. The highest O/C ratio on the surface of AC indicated that it had the highest oxygen content and thus the strongest hydrophilicity, which was very favorable for the removal of MB from the solution. Nitric acid treatment failed to increase the O/C ratio of the material surface, which is different from the results of previous studies (Gokce and Aktas, 2014), and may be due to the difference in reaction conditions. The higher O/C ratio of AC may be another key factor for its better MB removal performance.

As an oxygen-containing functional group, the high electron cloud

Table 4

The maximum adsorption capacities of various reported adsorbents for MB in the literature.

Adsorbent	pH	Temp (°C)	Time (min)	q_{\max} (mg/g)	References
Lignite modified by magnesium salts	7	50	240	149.0	(Bai et al. 2023a)
Corn husk	4	25	80	462.96	(Khodaie et al. 2013)
Neem bark (acid Treated)	–	25	–	47.62	(Tiwari, Singh, and Sharma 2015)
Soyabean dreg	9	45	120	1273.51	(Ying et al. 2021)
Bean activated by KOH	9	25	30	45.45	(Kahoul et al. 2019)
Coal on activation with KOH	–	30	240	200	(Jawad et al. 2018)
Activated carbon	5.6	30	290	491.7	(Jawad et al. 2019)
Pineapple peel	–	30	–	462.1	(Foo and Hameed 2012)
oil palm fiber	–	–	–	312.5	(Foo and Hameed 2011)
magnetic humic acid/graphene oxide composite	6	45	180	95.00	(Li et al. 2021)
This study	–	45	120	2040.696	

Table 5

The thermodynamic parameters of MB adsorption on AC.

ΔG^0 (KJ·mol ⁻¹)			ΔH^0 (KJ·mol ⁻¹)	ΔS^0 (J·(K·mol) ⁻¹)
298K	308K	318K	4.781	91.936
-22.610	-23.032	-85.869		

density of the carboxyl group makes it easy to form hydrogen bonds (Zhang et al., 2015). Hydrogen bonding plays an important role in MB adsorption process (Cao et al., 2023). To show the chemical bonding state of the elements on the surface of the materials more clearly, the high-resolution spectra of C 1 s (Fig. 6a) and O 1 s (Fig. 6b) of the three materials as well as the AC with adsorbed MB were split-peak fitted. The results showed that the intensities and positions of the attributed peaks, including the carboxyl groups, changed before and after the adsorption of MB on the AC, which indicated that the adsorption of MB changed the chemical environments of the elements C and O. The AC contained a higher proportion (8.70 % higher) of carboxyl groups than ACN (Fig. 6b), which may be another reason why the AC had a better removal effect on MB.

The nitrogen-containing functional groups on the surface of the material also played a positive role in the adsorption of hydrophilic dyes (Zheng et al., 2023). From the XPS gross spectral analysis (Table 1S), AC and ACN contain a higher proportion of nitrogen-containing groups than LC. This is one of the reasons for activation modification enhancing MB adsorption performance. The presence of basic nitrogen atoms provided a large number of active sites (Lian et al., 2016). The results were obtained by fractionally fitting the fine spectra of nitrogen-containing groups of AC and ACN, which are shown in Fig. 7. It can be seen that AC contains three basic nitrogen-containing functional groups, namely, amino (–NH₂), amine (–NH) and pyridine, which accounted for 83.21 % of the total nitrogen, with only 16.79 % being acidic graphite N. In contrast, the basic nitrogen-containing functional groups of ACN, amino (–NH₂) and amine (–NH), accounted for 62.93 %, while the percentage of the acidic N-containing functional group increased to 19.31 %, and oxidized N appeared. This may be another reason why AC is more effective in removing MB than ACN.

To summarize, AC showed better MB adsorption compared to ACN, which may be attributed to multiple factors such as the limitation of the molecular sieve effect, the increase in the content of oxygen-containing functional groups, the influence of carboxyl groups, and the role of nitrogen-containing functional groups.

3.6. Adsorption process

Numerous elements must be taken into account in the adsorption mechanism, including the kind of adsorbent, its molecular structure, its surface chemical characteristics, and the interactions between its functional groups. The adsorption of MB on AC is caused via pore stuffing, hydrogen bonding, π - π interactions, and electrostatic attraction (Guo and Du, 2012).

The function of AC's rich hierarchical porous structure in adsorption performance is illustrated in Fig. 8a. Capillary action is encouraged by pores, which also cooperatively move MB molecules into the porous structure of AC (Liu et al., 2023). The conjugated structure in AC and the benzene ring in MB molecules interact via π - π interactions, as depicted in Fig. 8b. Due to its high electronegativity, nitrogen has a major effect on AC surface electron density. Nitrogen atoms reduce the density of electrons on the surface of AC, hastening the process of π electron acceptance (Lin et al., 2020). The peak corresponding to C–C/C=C is found to significantly deviate towards higher binding energy (284.03 eV – 284.14 eV) when MB is adsorbed by AC. This is caused by electron transfer and a decrease in electron density. This provides more evidence that an electron donor–acceptor interaction occurs during the adsorption phase between π systems.

The role of electrostatic pull in MB molecule adsorption is illustrated

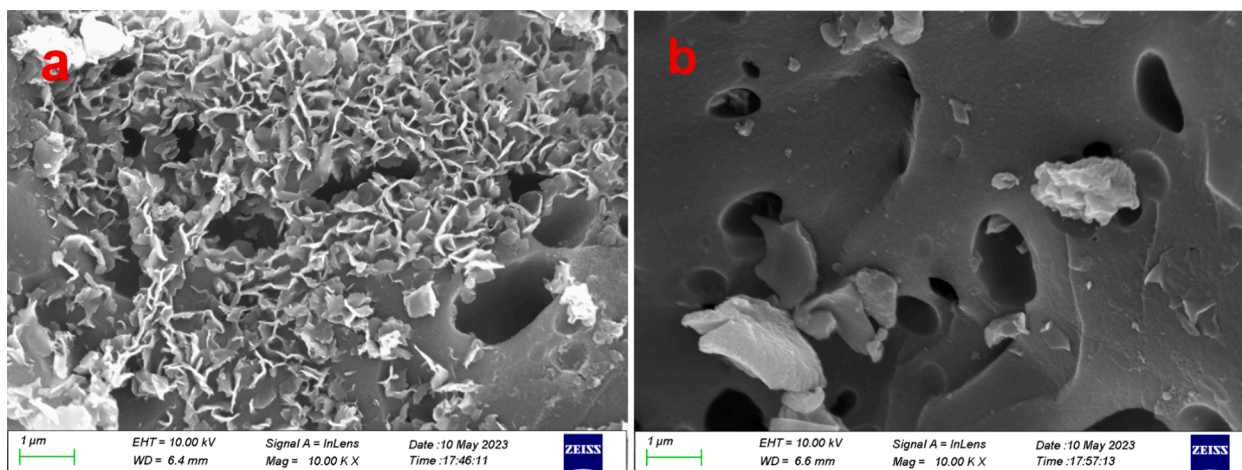


Fig. 4. SEM images:(a) AC-MB; (b) ACN-MB.

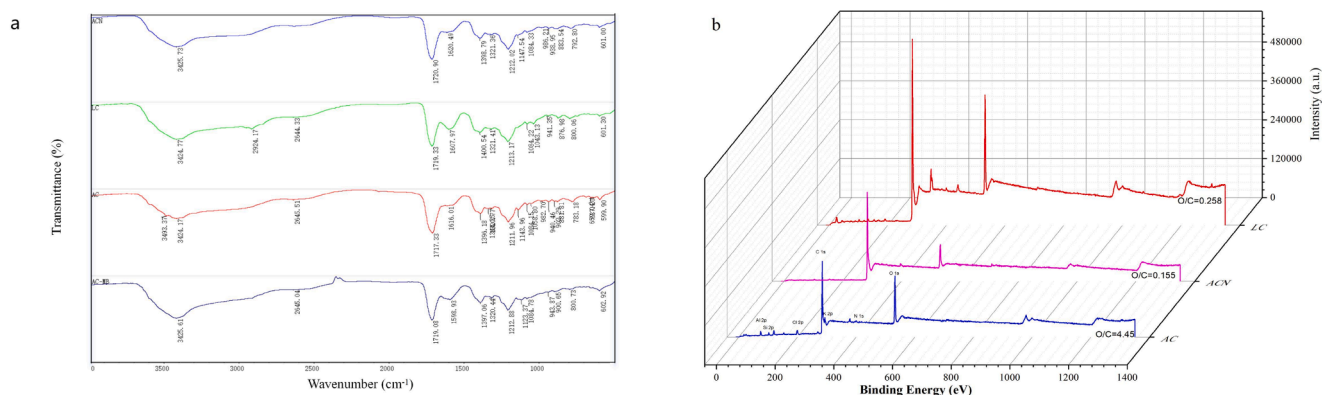


Fig. 5. (a)FTIR spectra of the samples; (b)XPS full spectra of the samples.

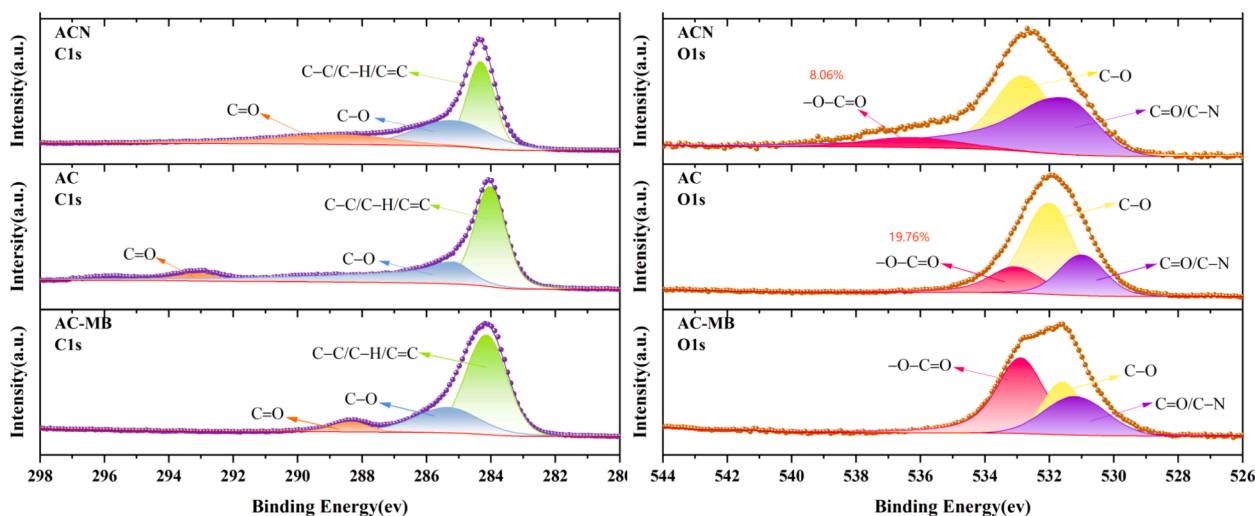


Fig. 6. The peak fitting results of the high-resolution XPS spectrum of the sample: (a)C 1 s and (b)O 1 s.

in Fig. 8c. The electrostatic interactions are reflected in the pH, which affects the capacity of AC to adsorb MB. The interactions of hydrogen bonds between MB and certain chemical groups of AC, namely carboxyl groups, are depicted in Fig. 8d. The size and binding energy of the peaks in the C 1 s and O 1 s fine modes change dramatically after AC adsorbs MB, suggesting that hydrogen bonds are formed during the adsorption process (Hussain et al., 2018).

4. Conclusion

In this study, we thoroughly investigated the efficient performance of AC in the removal of MB. The results demonstrate that AC significantly outperforms ACN in terms of adsorption efficiency. This advantage is primarily attributed to the 2–4 nm mesoporous structure of AC and its abundance of carboxyl and acidic nitrogen-containing functional groups. These properties are crucial in the adsorption process, facilitating hydrogen bonding, pore filling, electrostatic attraction, and π - π interactions.

Various factors affecting the adsorption of MB by AC, including adsorbent dosage, contact time, temperature, initial MB concentration, and pH, were systematically analyzed. Adsorption kinetic studies revealed that the adsorption process of MB on AC can be divided into three stages: fast adsorption, slow adsorption, and equilibrium. The high fit ($R^2 > 0.956$) of the pseudo-first-order and pseudo-second-order kinetic models indicated both physical and chemical characteristics of the adsorption process. The internal diffusion model's fitting results further confirmed the importance of internal diffusion and surface adsorption,

with the pseudo-second-order kinetic model providing a more accurate description of the adsorption behavior and showing a high consistency between the predicted equilibrium adsorption capacity and the experimental values.

Adsorption isotherm analysis indicated that the adsorption behavior of AC was consistent with the Langmuir model, with a maximum adsorption capacity at 318 K of 2040.696 mg/g, significantly higher than that of other adsorbents. Thermodynamic analyses demonstrated that the adsorption process of MB by AC was spontaneous, endothermic, and accompanied by an increase in entropy. The adsorption efficiency of AC was significantly improved with increasing temperature, as confirmed by the calculations of ΔG , ΔH , and ΔS .

Additionally, AC exhibited excellent adsorption efficiency and stability even after multiple uses and regeneration cycles. Regeneration experiments using anhydrous ethanol showed that the adsorption performance of AC only slightly decreased after five regeneration cycles, maintaining over 90 % MB removal efficiency, which proves its feasibility and regeneration capability for practical applications.

In conclusion, AC prepared from low-cost blue coke shows significant potential for MB removal, not only due to its efficient adsorption performance but also because of its good regeneration ability, making it highly suitable for industrial applications. This study provides a solid theoretical foundation and technical support for the application of blue coke-based modified activated carbon in wastewater treatment, and it reveals its broad application prospects in the field of environmental protection. Future studies will further explore the application potential of AC in removing various pollutants and optimize the preparation

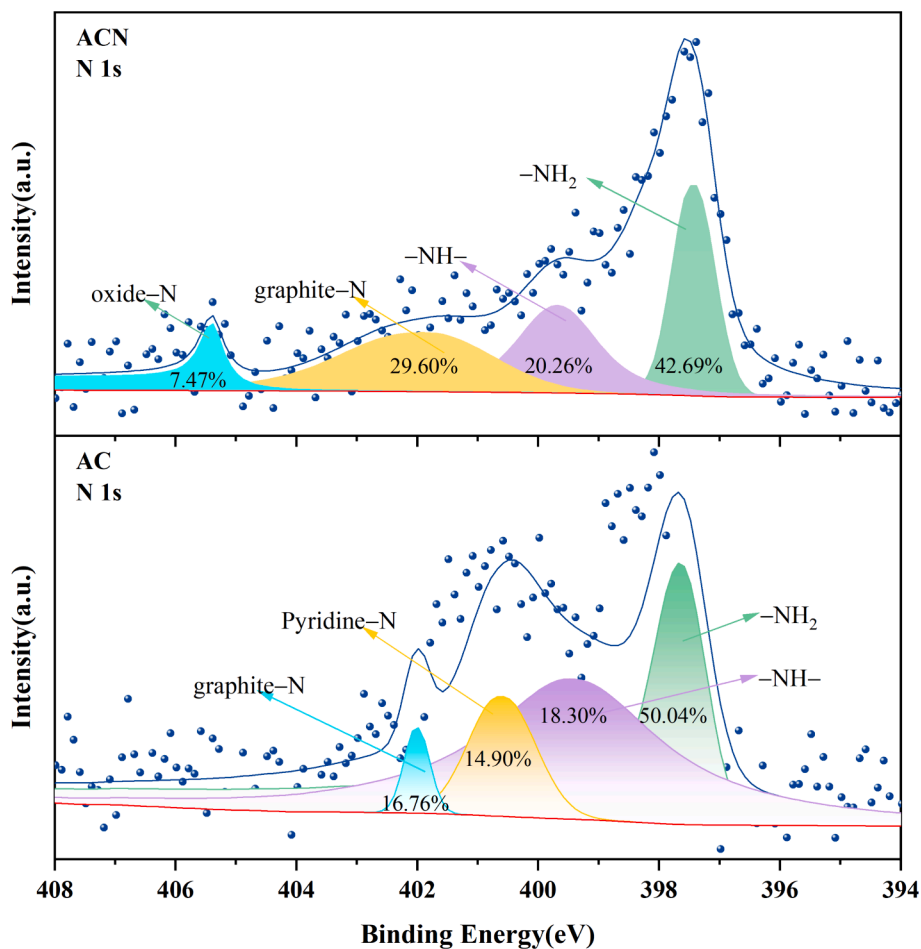


Fig. 7. Results of N 1 s peak fitting.

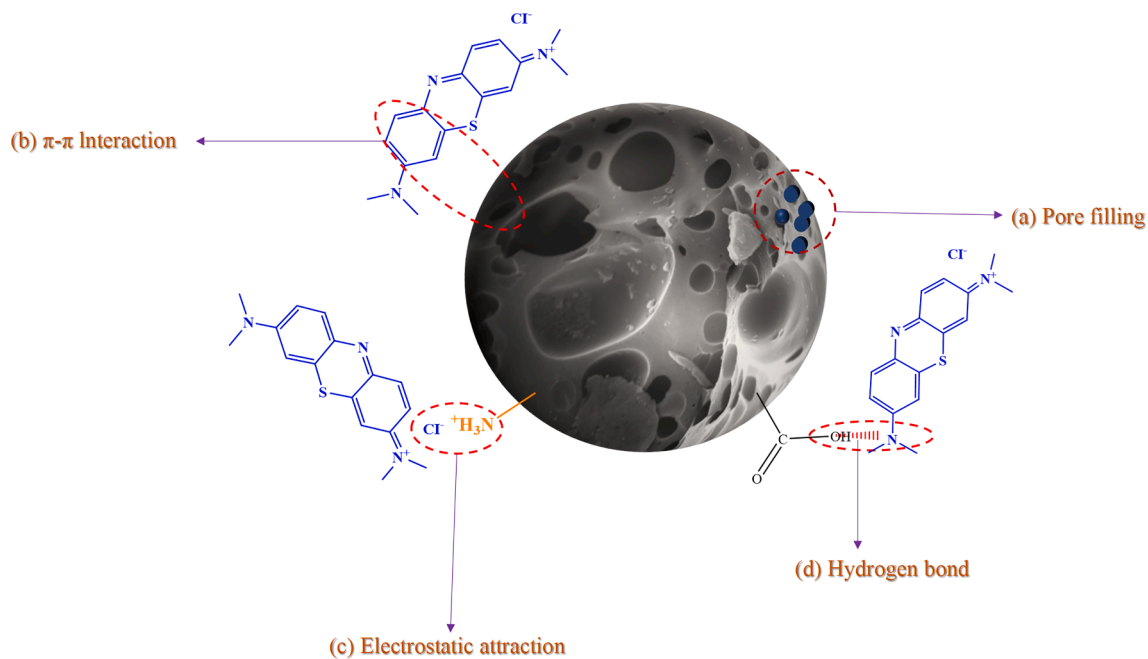


Fig. 8. Adsorption mechanism diagram of AC for MB.

process to enhance its practical effects in environmental remediation.

CRedit authorship contribution statement

Yunxuan Luoyang: Writing – original draft. **Hua Wang:** Writing – review & editing, Funding acquisition. **Wang Yong:** Resources. **Jian Li:** Funding acquisition. **Xia Li:** Data curation. **Han Shenghu:** Resources. **Nie Ying:** Resources. **Zhang Guotao:** Formal analysis.

Declaration of competing interest

The authors declare that they have no known competing financial interests or personal relationships that could have appeared to influence the work reported in this paper.

Data availability

Data is provided within the manuscript or [supplementary information files](#).

Acknowledgements

The authors would like to extend their heartfelt gratitude to the following funding sources for their generous financial support in facilitating this research project: National Natural Science Foundation of China (Grant No. 22168043), Key Scientific Research Program of the Shaanxi Provincial Department of Education (Project No. 23JS064 and 21JS047), Graduate Student Innovation Fund Project (Project No. 2023YLYCX12), Joint Project between Yulin University and the Chinese Academy of Sciences (Project No. YLUDNL202201), and Science and Technology Research and Development Project of the Yulin Science and Technology Bureau (Project No. CXY-2022-82). The invaluable support provided by these organizations has made a significant contribution to the successful completion of this study.

Appendix A. Supplementary material

Supplementary data to this article can be found online at <https://doi.org/10.1016/j.arabjc.2024.105898>.

References

- Alamin, U.I., Noor, A.S., Khan, A.N., Iqbal, J., Ullah, Z., Din, I.U., Muhammad, N., Khan, S.Z., 2021. Activated carbon-alginate beads impregnated with surfactant as sustainable adsorbent for efficient removal of methylene blue. *Int. J. Biol. Macromol.* 176, 233–243.
- Arabzadeh, M., Eslamidoost, Z., Rajabi, S., Hashemi, H., Aboulfotouh, A., Rosti, F., Nazari, F., Borj, B.P., Hajivand, M., 2023. Wastewater quality index (WWQI) as an indicator for the assessment of sanitary effluents from the oil and gas industries for reliable and sustainable water reuse. *Groundw. Sustain. Dev.* 23, 101015.
- Bai, R., Feng, Y., Lei, Wu., Li, Na., Liu, Q., Teng, Y., He, R., Zhi, K., Zhou, H., Qi, X., 2023a. Adsorption mechanism of methylene blue by magnesium salt-modified lignite-based adsorbents. *J. Environ. Manage.* 344, 118514.
- Bai, R., Feng, Y., Lei, Wu., Li, Na., Liu, Q., Teng, Y., He, R., Zhi, K., Zhou, H., Qi, X., 2023b. Adsorption mechanism of methylene blue by magnesium salt-modified lignite-based adsorbents. *J. Environ. Manage.* 344.
- Basta, A.H., Lotfy, V.F., Hasanin, M.S., Trens, P., El-Saied, H., 2019. Efficient treatment of rice byproducts for preparing high-performance activated carbons. *J. Clean. Prod.* 207, 284–295.
- Bello, Olugbenga Solomon, Idowu Abideen Adeogun, John Chijioke Ajaelu, Ezekiel Oluwaseun %J Chemistry Fehintola, and Ecology. 2008. 'Adsorption of methylene blue onto activated carbon derived from periwinkle shells: kinetics and equilibrium studies', 24: 285-95.
- Bouchelkia, N., Tahraoui, H., Amrane, A., Belkacemi, H., Bollinger, J.-C., Bouzaza, A., Zoukel, A., Zhang, J., Mouni, L., 2023. Jujube stones based highly efficient activated carbon for methylene blue adsorption: Kinetics and isotherms modeling, thermodynamics and mechanism study, optimization via response surface methodology and machine learning approaches. *Process Saf. Environ. Prot.* 170, 513–535.
- Cao, W. P., D. N. Li, S. S. Zhang, J. Ren, X. N. Liu, and X. H. Qi. 2023. 'Synthesis of hierarchical porous carbon sphere via crosslinking of tannic acid with Zn for efficient adsorption of methylene blue', *Arabian Journal of Chemistry*, 16.
- Chang, S.-K., Abbasi, Q.-u.-A., Abbasi, Z., Khushbakht, F., Ullah, I., Rehman, F.U., Hafeez, M., 2024. Rapid pH-dependent photocatalytic degradation of Methylene Blue by CdS nanorods synthesized through hydrothermal process. *Arab. J. Chem.* 17, 105422.
- Deng, Jiaqin, Yunan Liu, Hui Li, Zhongliang Huang, Xiaoli Qin, Jing Huang, Xuan Zhang, Xiaodong Li, and Qiang Lu. 2022. 'A novel biochar-copolymer composite for rapid Cr (VI) removal: Adsorption-reduction performance and mechanism', *SEPARATION AND PURIFICATION TECHNOLOGY*, 295.
- Elsherbiny, A.S., El-Hefnawy, M.E., Gemeay, A.H., 2017. Linker impact on the adsorption capacity of polyaspartate/montmorillonite composites towards methyl blue removal. *Chem. Eng. J.* 315, 142–151.
- Emmanuel, Ss., and Aa. Adesibikan. 2021. 'Bio-fabricated green silver nano-architecture for degradation of methylene blue water contaminant: A mini-review', *Water environment research : a research publication of the Water Environment Federation*.
- Feng, Y., Shaoping, Xu., 2020. Blue-coke production technology and the current state-of-the-art in China. *Carbon Resour. Convers.* 3.
- Feng, Y., Shaoping, Xu., Wang, K., 2024. Pyrolysis of shenmu coal to prepare blue-coke used as reductant. *J. Anal. Appl. Pyrol.* 180.
- Foo, K.Y., Hameed, B.H., 2011. Microwave-assisted preparation of oil palm fiber activated carbon for methylene blue adsorption. *Chem. Eng. J.* 166, 792–795.
- Foo, K.Y., Hameed, B.H., 2012. Porous structure and adsorptive properties of pineapple peel based activated carbons prepared via microwave assisted KOH and K₂CO₃ activation. *Micropor. Mesopor. Mater.* 148, 191–195.
- Gokce, Y., Aktas, Z., 2014. Nitric acid modification of activated carbon produced from waste tea and adsorption of methylene blue and phenol. *Appl. Surf. Sci.* 313, 352–359.
- Guo, Y., Erdeng, Du., 2012. The effects of thermal regeneration conditions and inorganic compounds on the characteristics of activated carbon used in power plant. *Energy Procedia* 17, 444–449.
- Guzel, F., Saygili, H., Saygili, G.A., Koyuncu, F., Yilmaz, C., 2017. Optimal oxidation with nitric acid of biochar derived from pyrolysis of weeds and its application in removal of hazardous dye methylene blue from aqueous solution. *J. Clean. Prod.* 144, 260–265.
- Han, Lin, Tingting Wang, Jianchao Gong, Xin Li, Yaxiong Ji, and Shifeng Wang. 2022. 'Multi-hydroxyl containing organo-vermiculites for enhanced adsorption of coexisting methyl blue and Pb(II) and their adsorption mechanisms', *COLLOIDS AND SURFACES A-PHYSICOCHEMICAL AND ENGINEERING ASPECTS*, 650.
- He, C., Liu, Z., Yun, Lu., Huang, L., Yang, Y., 2016. Graphene-supported silver nanoparticles with high activities toward chemical catalytic reduction of methylene blue and electrocatalytic oxidation of hydrazine. *Int. J. Electrochem. Sci.* 11, 9566–9574.
- Hu, Z., Guo, C., Wang, P., Guo, R., Liu, X., Tian, Y.e., 2022. Electrochemical degradation of methylene blue by Pb modified porous SnO₂ anode. *Chemosphere* 305, 135447.
- Huang, S., Pang, H., Li, L., Jiang, S., Wen, T., Zhuang, L.i., Baowei, Hu., Wang, X., 2018. Unexpected ultrafast and high adsorption of U(VI) and Eu(III) from solution using porous Al₂O₃ microspheres derived from MIL-53. *Chem. Eng. J.* 353, 157–166.
- Hussain, I., Li, Y., Qi, J., Li, J., Wang, L., 2018. Nitrogen-enriched carbon sheet for Methyl blue dye adsorption. *J. Environ. Manage.* 215, 123–131.
- Jawad, A.H., Mehdi, Z.S., Ishak, M.A.M., Ismail, K., 2018. Large surface area activated carbon from low-rank coal via microwave-assisted KOH activation for methylene blue adsorption. *Desalin. Water Treat.* 110, 239–249.
- Jawad, A.H., Ismail, K., Ishak, M.A.M., Wilson, L.D., 2019. Conversion of Malaysian low-rank coal to mesoporous activated carbon: Structure characterization and adsorption properties. *Chin. J. Chem. Eng.* 27, 1716–1727.
- Jawad, A.H., Sahu, U.K., Jani, N.A., Alothman, Z.A., Wilson, L.D., 2022. Magnetic crosslinked chitosan-tripolyphosphate/MgO/Fe₃O₄ nanocomposite for reactive blue 19 dye removal: Optimization using desirability function approach. *Surfaces Interfaces* 28.
- Kahoul, I., Bougdah, N., Djazi, F., Djilani, C., Magri, P., Medjram, M.S., 2019. Removal of methylene blue by adsorption onto activated carbons produced from agricultural wastes by microwave induced KOH activation. *Ch&ChT* 13, 365–371.
- Khasri, A., Bello, O.S., Ahmad, M.A., 2018. Mesoporous activated carbon from <i>Pentace</i> species sawdust via microwave-induced KOH activation: optimization and methylene blue adsorption. *Res. Chem. Intermed.* 44, 5737–5757.
- Khodaie, M., Ghasemi, N., Moradi, B., Rahimi, M., 2013. Removal of methylene blue from wastewater by adsorption onto znclactivated corn husk carbon equilibrium studies. *J. Chem.*
- Küçük, İ., 2023. Improvement of methylene blue adsorption properties of lemon peel by surface modification. *Chem. Data Collect.* 46, 101042.
- Li, D., Hua, T., Yuan, J., Feigao, Xu., 2021. Methylene blue adsorption from an aqueous solution by a magnetic graphene oxide/humic acid composite. *Colloids Surf. A Physicochem. Eng. Asp.* 627, 127171.
- Li, H., Jiang, D., Huang, Z., He, K., Zeng, G., Chen, A., Yuan, L., Peng, M., Huang, T., Chen, G., 2019. Preparation of silver-nanoparticle-loaded magnetic biochar/poly (dopamine) composite as catalyst for reduction of organic dyes. *J. Colloid Interface Sci.* 555, 460–469.
- Lian, F., Cui, G.N., Liu, Z.Q., Duo, L., Zhang, G.L., Xing, B.S., 2016. One-step synthesis of a novel N-doped microporous biochar derived from crop straws with high dye adsorption capacity. *J. Environ. Manage.* 176, 61–68.
- Lin, R., Liang, Z., Yang, C., Zhao, Z., Cui, F., 2020. Selective adsorption of organic pigments on inorganically modified mesoporous biochar and its mechanism based on molecular structure. *J. Colloid Interface Sci.* 573, 21–30.
- Liu, Chao, A. M Omer, and Xiao-kun Ouyang. 2017. 'Adsorptive removal of cationic methylene blue dye using carboxymethyl cellulose/k-carrageenan/activated montmorillonite composite beads: Isotherm and kinetic studies', *International Journal of Biological Macromolecules*: 823-33.

- Liu, B., Lv, P., Ruofei, Wu., Bai, Y., Wang, J., Weiguang, Su., Song, X., Guangsu, Yu., 2023. Coal gasification fine slag based multifunctional nanoporous silica microspheres for synergistic adsorption of Pb(II) and Congo red. *Separ. Purif. Technol.* 323, 124478.
- Lu, J., Zahedi, A., Yang, C., Wang, M., Peng, B.o., 2013. Building the hydrogen economy in China: Drivers, resources and technologies. *Renew. Sustain. Energy Rev.* 23, 543–556.
- Makhado, E., Pandey, S., Nomngongo, P.N., Ramontja, J., 2017. Preparation and characterization of xanthan gum-cl-poly(acrylic acid)/o-MWCNTs hydrogel nanocomposite as highly effective re-usable adsorbent for removal of methylene blue from aqueous solutions. *J. Colloid Interface* 700–714.
- Malatji, Nompumelelo, Edwin Makhado, Kwena D. Modibane, Kabelo E. Ramohlola, Thabiso C. Maponya, Gobeng R. Monama, and Mpitloane J. Hato. 2021. 'Removal of methylene blue from wastewater using hydrogel nanocomposites: A review', *Nanomaterials and Nanotechnology*, 11: 18479804211039425.
- Mani, D., Duraisamy Elango, A., Priyadharsan, L.A., Al-Humaid, N.D., Al-Dahmash, S., Ragupathy, P.J., Ahn, Y.-H., 2023. Groundnut shell chemically treated with KOH to prepare inexpensive activated carbon: Methylene blue adsorption and equilibrium isotherm studies. *Environ. Res.* 231, 116026.
- Miao, Z., Guo, Z., Qiu, G., Zhang, Y., Jianjun, Wu., 2021. Synthesis of activated carbon from high-ash coal gasification fine slag and their application to CO₂ capture. *J. CO₂ Util.* 50.
- Nabilah, B., Purnomo, A.S., Prasetyoko, D., Rohmah, A.A., 2023. Methylene Blue biodecolorization and biodegradation by immobilized mixed cultures of *Trichoderma viride* and *Ralstonia pickettii* into SA-PVA-Bentonite matrix. *Arab. J. Chem.* 16, 104940.
- Parakala, S., Moulik, S., Sridhar, S., 2019. Effective separation of methylene blue dye from aqueous solutions by integration of micellar enhanced ultrafiltration with vacuum membrane distillation. *Chem. Eng. J.* 375, 122015.
- Sahu, U.K., Mandal, S., Sahu, S., Gouda, N., Patel, R.K., 2022. Preparation and characterization of mesoporous cerium oxide for toxic As(V) removal: Performance and mechanistic studies. *J. Environ. Eng. Landsc. Manag.* 30, 321–330.
- Sen, T.K., 2014. Review on dye removal from its aqueous solution into alternative cost effective and non-conventional adsorbents. *J. Chem. Process Eng.* 1, 1–7.
- Somyanonthanakun, W., Ahmed, R., Krongtong, V., Thongmee, S., 2023. Studies on the adsorption of Pb(II) from aqueous solutions using sugarcane bagasse-based modified activated carbon with nitric acid: Kinetic, isotherm and desorption. *Chem. Phys. Impact* 6, 100181.
- Sundaran, S.P., Reshmi, C.R., Sagitha, P., Manaf, O., Sujith, A., 2019. Multifunctional graphene oxide loaded nanofibrous membrane for removal of dyes and coliform from water. *J. Environ. Manage.* 240, 494–503.
- Teixeira, Yago Neco, Francisco José de Paula Filho, Vinícius Pereira Bacurau, Jorge Marcell Coelho Menezes, Anderson Zhong Fan, and Ricardo Paulo Fonseca Melo. 2022. 'Removal of Methylene Blue from a synthetic effluent by ionic flocculation', *Heliyon*, 8: e10868.
- Tian, Y., Ren, Q., Bai, X., Liu, B., Jing, X., Lan, X., 2022. Effect of direct coal liquefaction residue on the properties of fine blue-coke-based activated coke. *Green Process. Synth.* 11, 396–403.
- Tiwari, D.P., Singh, S.K., Sharma, N., 2015. Sorption of methylene blue on treated agricultural adsorbents: equilibrium and kinetic studies. *Appl. Water Sci.* 5, 81–88.
- Vasiraja, N., R. Saravana Sathiy Prabhakar, and A. Joshua. 2023. 'Preparation and Physio-Chemical characterisation of activated carbon derived from prosopis juliflora stem for the removal of methylene blue dye and heavy metal containing textile industry effluent', *JOURNAL OF CLEANER PRODUCTION*, 397.
- Wang, D., Wang, Z., Zheng, X., Tian, M., 2020. Activated carbon fiber derived from the seed hair fibers of *Metaplexis japonica*: Novel efficient adsorbent for methylene blue. *Ind. Crop. Prod.* 148.
- Wang, W., Wang, H., Luoyang, Y., Zhang, G., Gao, X., Li, J., Li, X., He, M., 2023. Nitric acid-treated blue coke-based activated carbon's structural characteristics and its application in hexavalent chromium-containing wastewater treatment. *Molecules* 28.
- Ying, Z., Chen, X., Li, H., Liu, X., Zhang, C., Zhang, J., Yi, G., 2021. Efficient adsorption of methylene blue by porous biochar derived from soybean dreg using a one-pot synthesis method. *Molecules* 26.
- Yong, Wang, L. I. Hu-Fei, A. N. Fu-Qiang, and School Of %J Applied Chemical Industry Science. 2019. 'Preparation of activated carbon based on hair and its selectively removing ability for Fe(III) in rare earth'.
- Yusop, Mohamad Firdaus Mohamad, Mohd Azmier Ahmad, Nur Ayshah Rosli, and Mohd Edeerozey Abd Manaf. 2021. 'Adsorption of cationic methylene blue dye using microwave-assisted activated carbon derived from acacia wood: Optimization and batch studies', *Arabian Journal of Chemistry*, 14.
- Zhang, W.L., Yin, J., Lin, Z.Q., Lin, H.B., Lu, H.Y., Wang, Y., Huang, W.M., 2015. Facile preparation of 3D hierarchical porous carbon from lignin for the anode material in lithium ion battery with high rate performance. *Electrochim. Acta* 176, 1136–1142.
- Zheng, Liang, Huimei Wang, Xiaohui Wang, Fangong Kong, Yu Liu, and Fengshan Zhang. 2023. 'Fabrication of N-doped micro-mesoporous carbons from industrial alkali lignin with urea assistance for high-efficiency adsorption of methylene blue', *Industrial Crops and Products*, 203: 117146.